CERN – EUROPEAN ORGANIZATION FOR NUCLEAR RESEARCH
CERN - AB DEPARTMENT

CTF3 Note 061 (Tech.)
(Beam Loss Detection)

CALCULATION OF BEAM LOSS INDUCED PARTICLE FLUX FOR CTF3

M. Wood, Northwestern University, Illinois, USA

Abstract

This report summarizes the results of a study to compute the beam loss induced particle flux outside the CTF3 accelerator vacuum chamber. GEANT 3.21 was used for all of the calculations in this study. The goal of this study is to better understand the beam loss environment for a high intensity electron beam like that at CTF3 or the proposed CLIC accelerator. Any future beam loss monitoring system will depend on an understanding of how beam losses translate to secondary particle fluxes.

Geneva, Switzerland
9 January 2004

Calculation of Beam Loss Induced Particle Flux for CTF3

Matthew Wood

January 8, 2004

1 Introduction

This report summarizes the results of a study to compute the beam loss induced particle flux outside the CTF3 accelerator vacuum chamber. GEANT 3.21 was used for all of the calculations in this study. The goal of this study is to better understand the beam loss environment for a high intensity electron beam like that at CTF3 or the proposed CLIC accelerator. Any future beam loss monitoring system will depend on an understanding of how beam losses translate to secondary particle fluxes.

1.1 Simulation Geometry

The simulations in this study were run with two different geometries. The first geometry is an idealized representation of a beam pipe section with no other surrounding structures. In the simulation, the beam pipe is represented by an iron tube of thickness 0.2 cm and outer diameter 4.45 cm. The second geometry is an idealized CTF3 drive beam linac module. Each module consists of two copper accelerating structures of length 114 cm, a triplet of quadrupole magnets each of length 20 cm, and one beam position monitor of length 10 cm. Those regions between these three structures are connected by beam pipe as described for the first simulation geometry. The total length of each linac module is 450 cm. In both simulations, the x and y axes form a transverse plane with respect to the linac while the z-axis corresponds to the longitudinal axis.

1.2 Representing Beam Loss

Beam loss will be an important consideration for CTF3 since the nominal drive beam intensity is 3.5 A. No attempt was made in this study to create a realistic model for beam loss. In each simulation, the beam loss was represented by introducing a mono-energetic beam of electrons at a single angle and position with respect to the geometry. Unless otherwise noted the beam loss occurs with an angle of 30 mrad at the intersection of the beam pipe or accelerating structure with the y-axis. The electrons have no momentum component in the x direction. Fluxes produced by the simulation were scaled with respect to a 1 ‰ loss of the beam which is 3.5 mA at nominal CTF3 intensity.

1.3 Characterizing Secondaries

The primary mechanism by which high energy electrons create secondaries is through the formation of electromagnetic showers. In an electromagnetic shower, a cascade develops as electrons or positrons emit bremsstrahlung photons which then can produce more electrons and positrons via pair production. Bremsstrahlung photons of energy greater than approximately 5 MeV can also

induce the production of secondary neutrons and pions. The cross-section for these processes is on average 10^{-3} times smaller than that for pair production. GEANT 3.21 does not simulate these interactions and thus fluxes of neutrons and other hadrons will not be presented in this study.

In this study no distinction is made between electrons and positrons since it is assumed that they will be seen in the same way by a beam loss detection system. Furthermore, a low energy cut-off of 100 keV was placed on the production of all secondary particles.

2 Beam Pipe Simulations

The primary goals of the beam pipe simulations were to understand how observed fluxes vary with the angle, energy, and position of the beam loss. The symmetry of this geometry allows a very general characterization of these behaviors.

2.1 Flux and Energy Distributions

Shown in Figure 1 are flux and energy distributions of beam loss secondaries for a beam energy of 25 MeV at an angle of 30 mrad and a distance of 100 cm from the point of beam loss. Because the linac modules are 450 cm in length, 100 cm is roughly of the order of the distance that we expect to have between beam loss and a beam loss detector.

As can be seen in the radial flux plot, the flux of photons is more than an order of magnitude greater than the flux of electrons. As seen from the energy distribution, this discrepancy is due primarily to the high flux of lower energy photons below 5 MeV. Both the photon and electron flux distributions form one high flux peak in the direction of beam loss and a smaller peak on the opposite side of the pipe.

Shown in Figure 2 are the same distributions as in Figure 1 with a beam energy of 100 MeV. The shape of all the distributions remains relatively similar while the total flux increases proportionally with the beam energy. At this beam energy, the flux peaks on either side of the beam pipe become less diffuse.

2.2 Flux Dependence on Beam Loss Angle

In order to see how the angle of incidence might affect secondary fluxes, two sets of simulations were run at beam energies of 25 and 100 MeV while varying the beam loss angle from 10 to 150 mrad. Shown in Figure 3 are Y projections of the flux distributions for photons and electrons. The observed shifts in these flux distributions demonstrate the effect of considering the transverse momentum distribution of the beam loss. A higher angle represents the behavior of beam losses that as a whole have a higher p_T and vice versa. As seen in Figure 3, small shifts in angle of the order of 20 mrad change the flux projection by 10-20 %. At higher angles, the second flux peak on the opposite side of the pipe from the beam loss gradually disappears. The positions of the two flux peaks shift only slightly with angle.

2.3 Flux Dependence on Beam Energy

The CTF3 drive beam linac will accelerate electrons from 24 to 150 MeV. The effect of the beam energy on secondary fluxes is thus an important consideration. Furthermore, the future CLIC accelerator will produce electrons with energies on the order of GeV and TeV. In Figure 4 are some

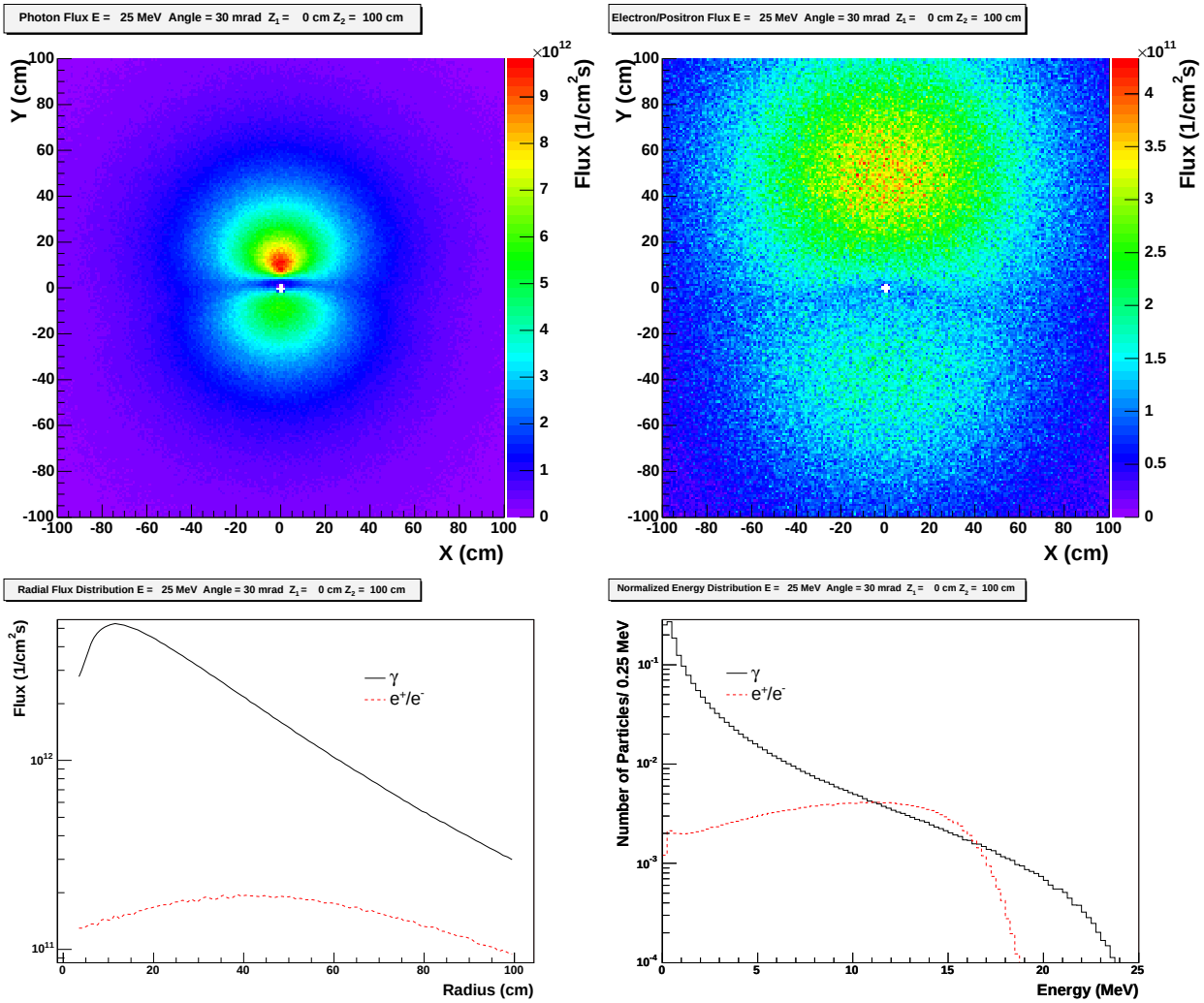

Figure 1: Flux and Energy Distributions for a beam energy of 25 MeV at a distance of 100 cm from the point of beam loss. This represents the initial energy of the CTF3 linac. All fluxes are normalized with respect to a beam loss intensity of 3.5 mA. The energy distribution in the lower right plot is normalized to a single electron.

comparisons of fluxes at beam energies in the range 25 - 1000 MeV. Although 150 MeV is the maximum beam energy for CTF3, it is useful to see how fluxes will scale at higher energies.

From the plots in Figure 4 one can see that the secondary fluxes scale roughly linearly with the beam energy. This is an important consideration because the beam energy will gradually increase along the length of the linac. The sensitivity of a beam loss detection system will need to be tuned to the energy of the beam in that particular section of the linac.

2.4 Flux Dependence on Distance

The task of a beam loss detection system will be to localize the point of beam loss by measuring the secondary fluxes. Thus it is useful to examine how the measured fluxes vary with the distance from the point of beam loss. Shown in Figure 5 are fluxes integrated over the azimuthal angle at

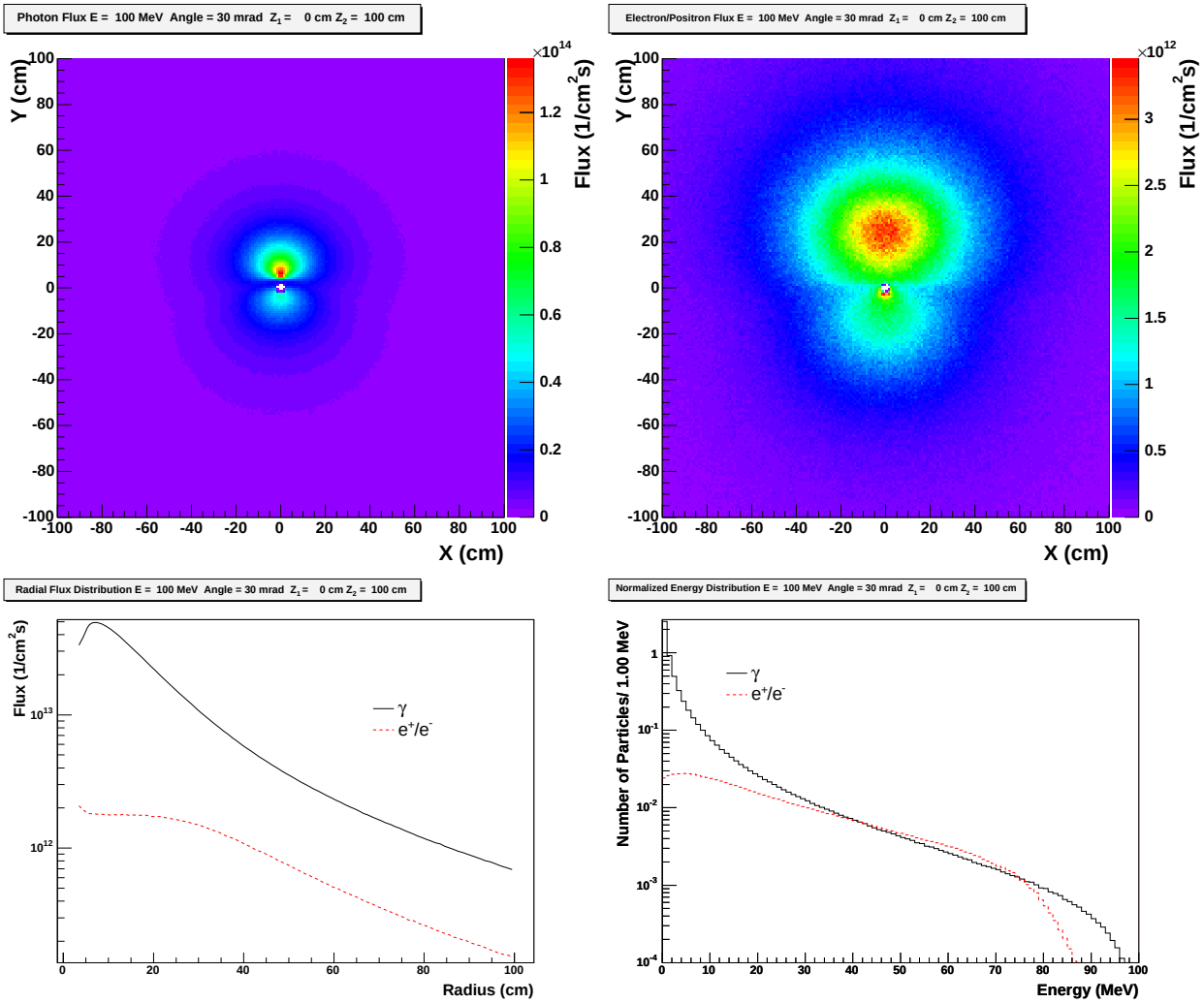

Figure 2: Flux and Energy Distributions for a beam energy of 100 MeV at a distance of 100 cm from the point of beam loss.

radii of 20 and 40 cm versus the distance from the beam loss. Based on these results, one could conceivably localize the point of beam loss to within 10-20 cm if one knew both the beam energy and beam loss intensity. As seen in these plots the flux of electrons is much more sensitive to the position of beam loss than the flux of photons.

3 Drive Beam Linac Simulations

The second geometry used in these simulations was that of the CTF3 drive beam linac (see Figure 6). Since the detailed structure of the linac does not have a large impact on the generation of secondaries, a simplified description of the linac geometry was used. The linac is composed of repeating modules each having a triplet of quadrupole magnets, two accelerating structures, and one beam position monitor. The z coordinate in these simulations was defined with respect to the center of the second magnet in the quadrupole triplet.

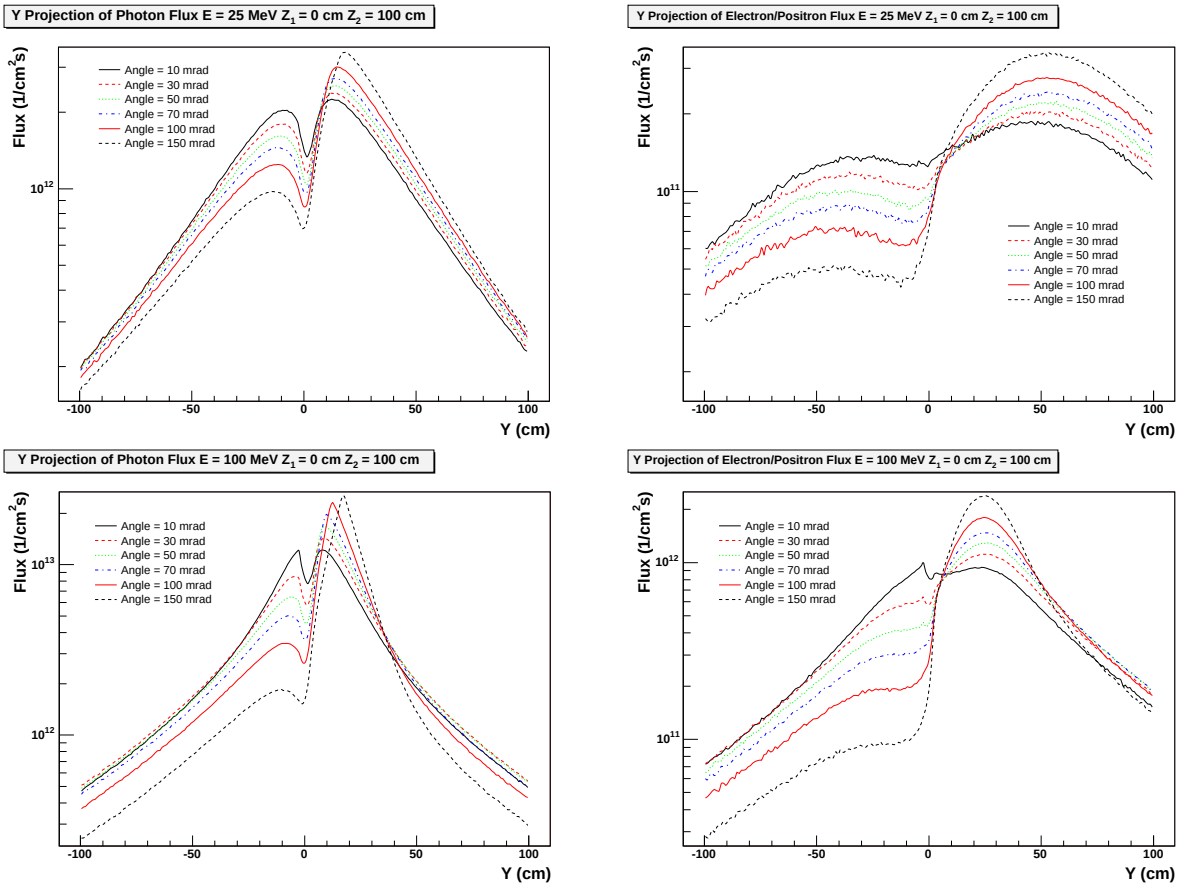

Figure 3: Y Projections of photon and electron/positron flux at 25 and 100 MeV. The six contours represent increasing beam loss angle from 10 to 150 mrad.

Because the structure of each drive beam linac module varies significantly along the z-axis, an important consideration is the position of beam loss along this axis. By design the beam size of the CTF3 drive beam linac will be largest near the quadrupole magnets and we expect to see the greatest beam losses there. Thus beam losses were simulated at four points along the linac geometry: at the center of each of the three quadrupole magnets (Z = -47, 0, 47 cm) and at the entrance to the first accelerating structure (Z = 98 cm) where the diameter of the beam line narrows from 40.5 mm to 34 mm. Fluxes were then simulated for positions that might be suitable for placing a beam loss detection system: between the second and third magnets (Z = 25 cm), before and after the entrance to the first accelerating structure (Z = 75, 120 cm), and at the center of the first accelerating structure (Z = 155 cm).

3.1 Flux and Energy Distributions

In Figure 7 is a comparison of the flux distributions for the beam pipe simulations and the drive beam linac simulations. As compared to the beam pipe simulations the flux of both photons and electrons is reduced by nearly an order of magnitude. There is also a significant screening effect created by the quadrupole magnet at Z = 47 cm. The outline of the magnet is clearly visible in the flux distribution and for this particular arrangement extends out to approximately 50 cm. Another effect of the quadrupole magnet is that the region of highest flux is actually on the opposite side of the geometry from which the beam loss occurred.

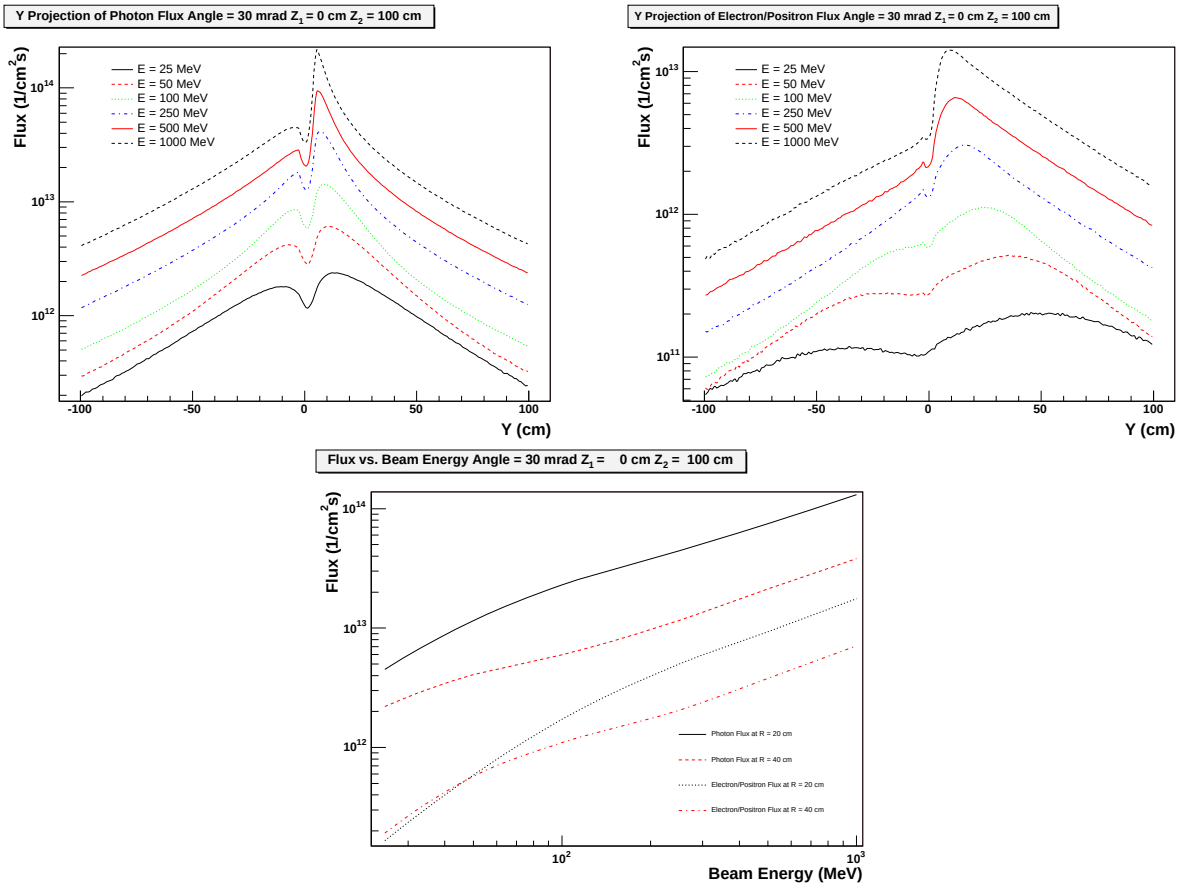

Figure 4: Y Projections of photon and electron/positron flux at a distance of 100 cm from the point of beam loss for beam energies from 25 to 1000 MeV.

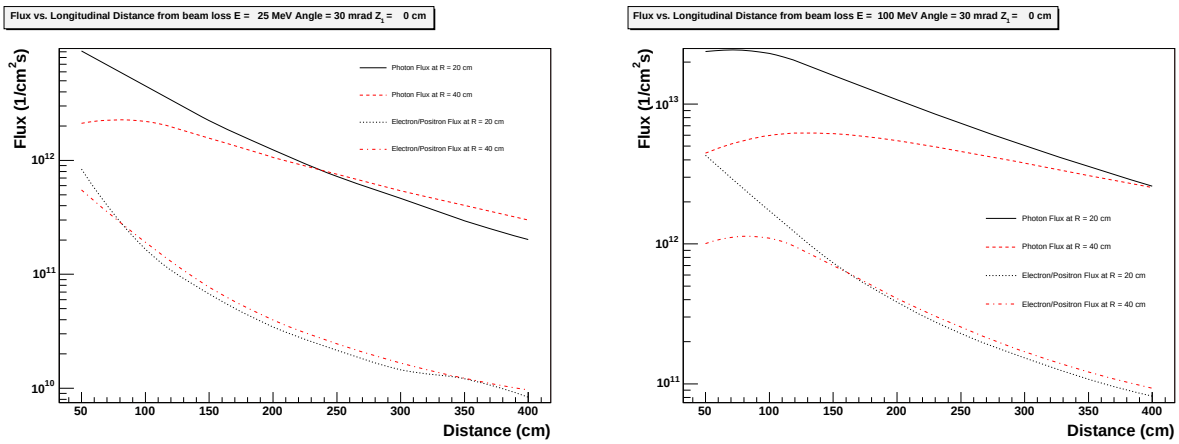

Figure 5: Average flux over an annulus at 20 and 40 cm at various distances from the point of beam loss.

In Figure 8 is a comparison of electron flux distributions using the linac geometry for four different longitudinal positions. Here one can more clearly see how the screening effect develops along the linac.

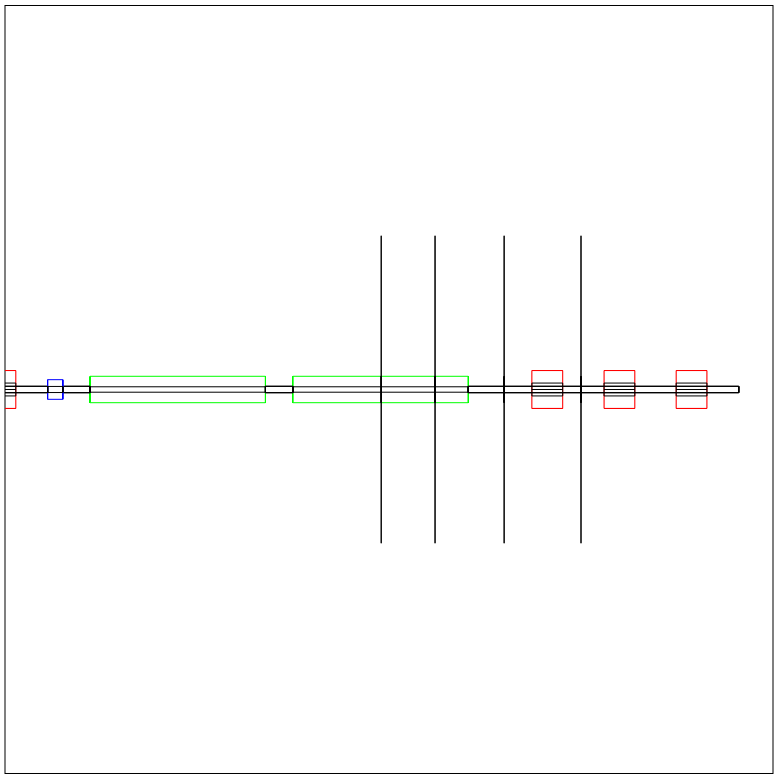

Figure 6: GEANT geometry used for the simulation of the CTF3 drive beam linac. The three linac structures represented in the geometry are the quadrupole magnets (red), accelerating structures (green) and beam position monitor (blue). The four vertical black lines represent the positions at which fluxes were measured.

3.2 Measuring Beam Loss Position and Intensity

Ultimately a beam loss detection system should be able to localize the position and intensity of beam loss within a single linac module. This task is relatively straightforward for the case of a simple beam pipe. The introduction of magnets and accelerating structures makes the task more complex because the observed signal depends not only on the distance from the beam loss but also on the intervening linac structures.

In Figure 9 is a comparison of flux projections at the center of the first accelerating structure (Z = 155 cm). Each projection represents a beam loss occurring at a different point on the linac module. While the flux projections at the three quadrupole magnets all scale with distance, the observed flux resulting from a loss at the first accelerating structure is actually less than that from a loss occurring at the first magnet which is nearly 150 cm away. This result suggests that it will be difficult to localize a loss occurring here since a sensitive detector will be overwhelmed by even a small loss occurring farther down the linac. Because it is necessary to be sensitive to both beam loss position and intensity, it will be important in the future to look at both the relative shape and magnitude of beam loss secondaries.

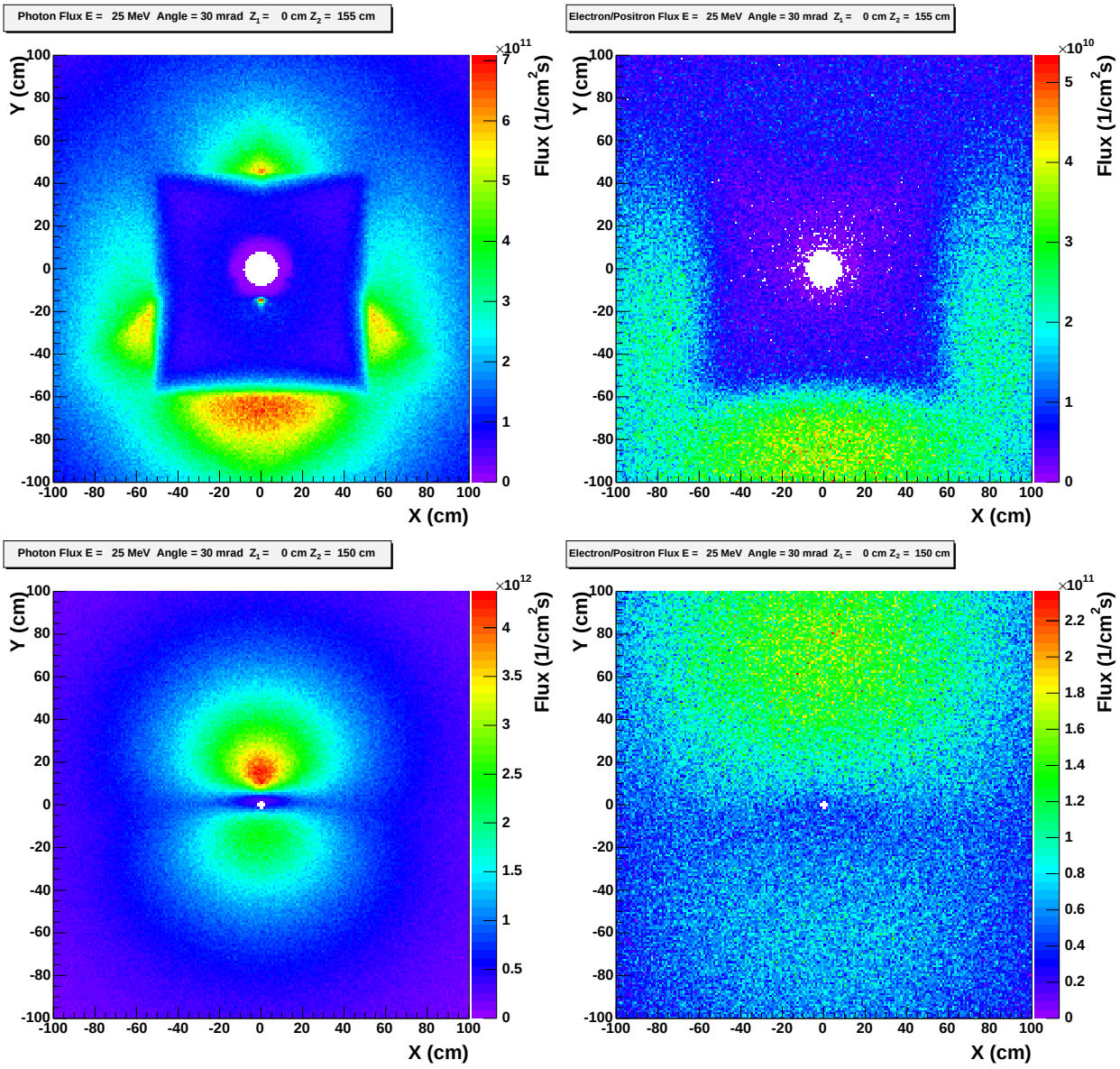

Figure 7: Comparison of flux distributions for beam pipe and linac simulations at a beam energy of 25 MeV and angle 30 mrad. The upper two plots give the linac simulation flux distributions at the center of the first accelerating structure (Z = 155 cm) for a beam loss occurring at the center of the second quadrupole magnet (Z = 0 cm). The lower two plots give the beam pipe simulation flux distributions at approximately the same distance from the beam loss (Z = 150 cm).

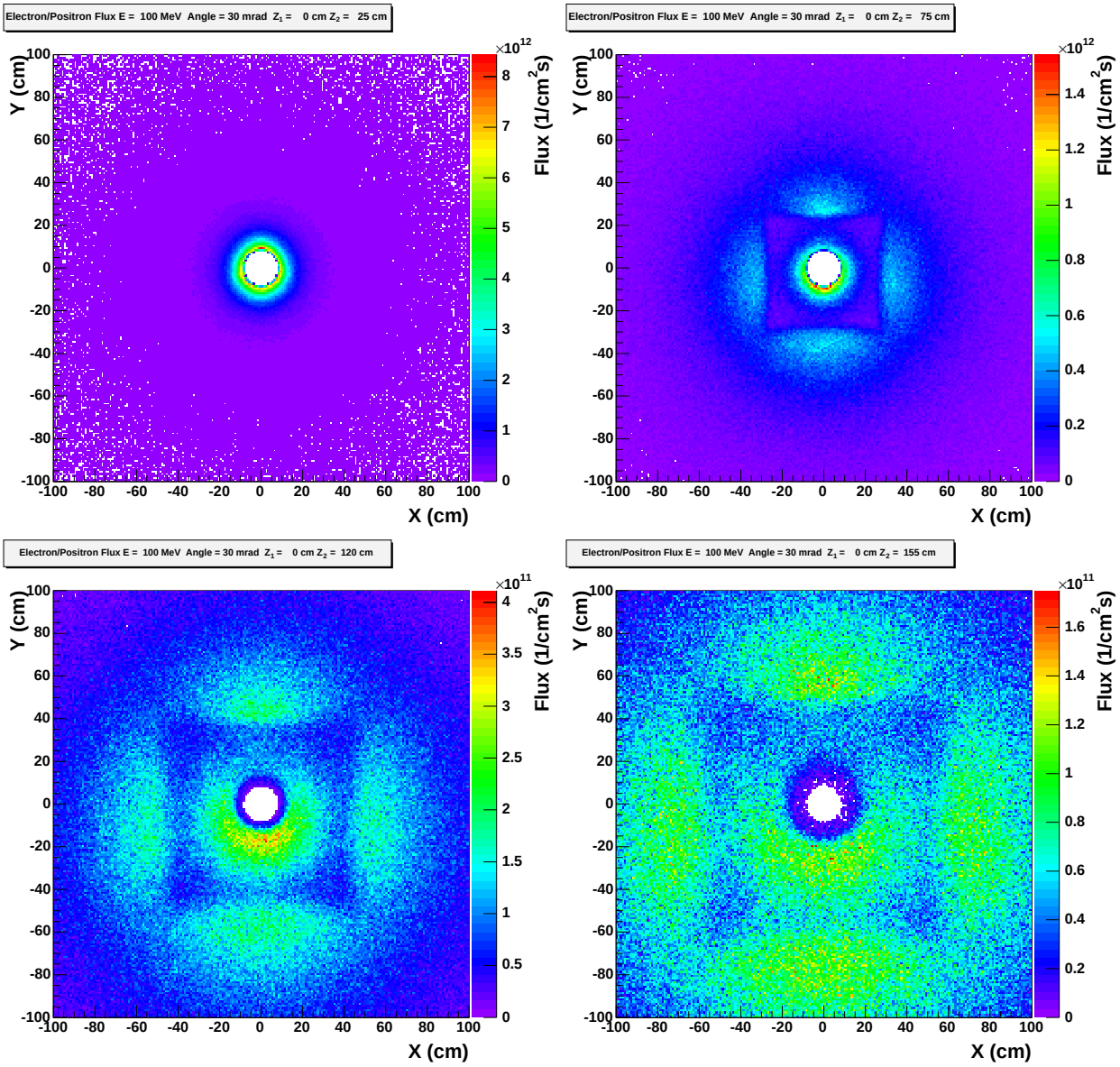

Figure 8: Comparison of linac simulation electron flux distributions at a beam energy of 100 MeV and angle 30 mrad. The four distributions represent four different longitudinal positions (Z = 25, 75, 120, 155 cm) with a beam loss occurring at the center of the second quadrupole magnet (Z = 0 cm).

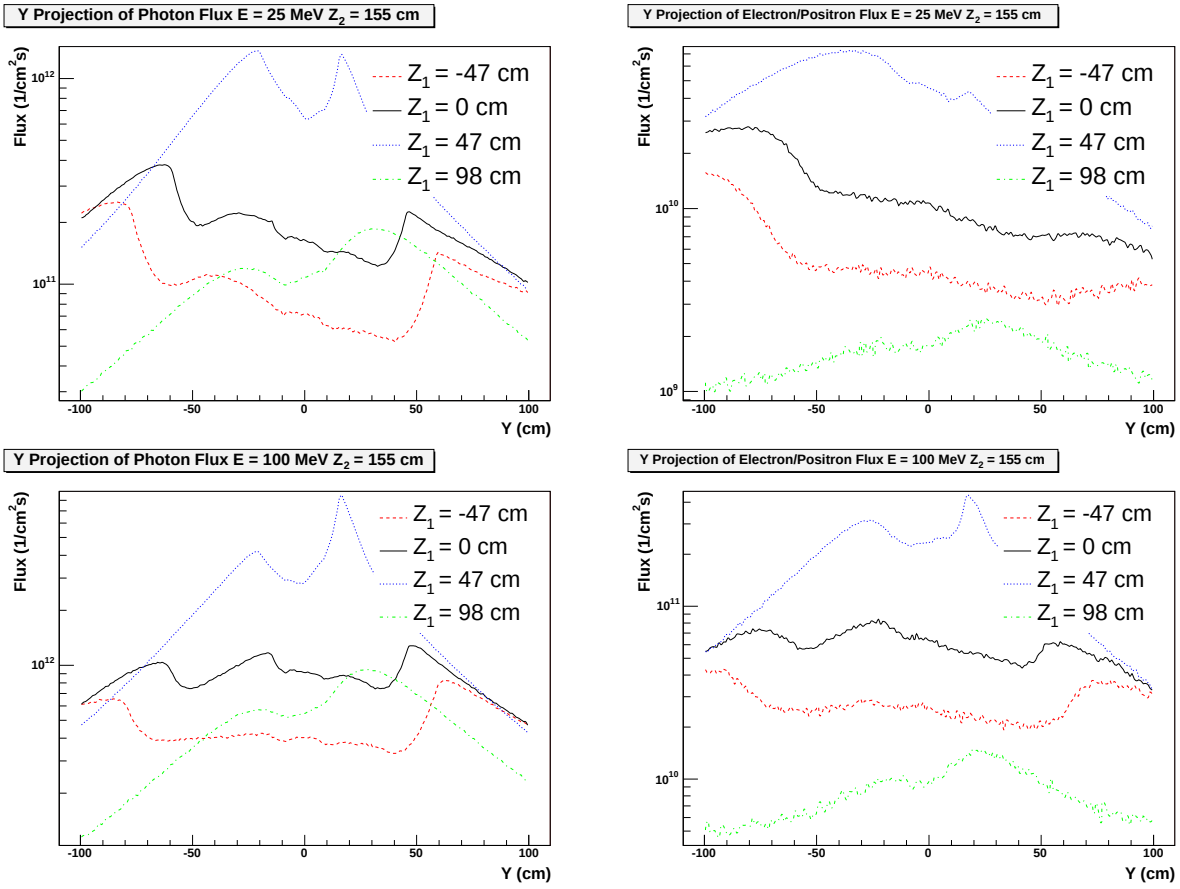

Figure 9: Comparison of photon and electron fluxes at Z = 155 cm for beam energies of 25 and 100 MeV and beam losses at four points along the linac. Here one can estimate how difficult it would be discriminate the point of beam loss by looking at the flux projection alone.